

Published in final edited form as:

*Magn Reson Med.* 2009 December ; 62(6): 1523–1532. doi:10.1002/mrm.22142.

## 3D Noncontrast MR Angiography of the Distal Lower Extremities Using Flow-Sensitive Dephasing (FSD)-Prepared Balanced SSFP

Zhaoyang Fan<sup>1,2</sup>, John Sheehan<sup>1</sup>, Xiaoming Bi<sup>3</sup>, Xin Liu<sup>1</sup>, James Carr<sup>1</sup>, and Debiao Li<sup>1,2,\*</sup>

<sup>1</sup> Department of Radiology, Northwestern University, Chicago, Illinois, USA

<sup>2</sup> Department of Biomedical Engineering, Northwestern University, Evanston, Illinois, USA

<sup>3</sup> Siemens Medical Solutions USA, Inc., Chicago, Illinois, USA

### Abstract

While three-dimensional contrast-enhanced MR angiography (MRA) is becoming the method of choice for clinical peripheral arterial disease (PAD) examinations, safety concerns with contrast administration in patients with renal insufficiency have triggered a renaissance of noncontrast MRA. In this work, a noncontrast-MRA technique using electrocardiography-triggered three-dimensional segmented balanced steady-state free precession with flow-sensitive dephasing (FSD) magnetization preparation was developed and tested in the distal lower extremities. FSD preparation was used to induce arterial flow voids at systolic cardiac phase while having little effect on venous blood and static tissues. High-spatial-resolution MRA was obtained by means of magnitude subtraction between a dark-artery scan with FSD preparation at systole and a bright-artery scan without FSD preparation at mid-diastole. In nine healthy volunteers, FSD parameters, including the gradient waveform and the first-order gradient moment, were optimized for excellent MRA image quality. Furthermore, arterial stenosis and occlusion in two peripheral arterial disease patients were identified using the noncontrast-MRA technique, as confirmed by contrast-enhanced MRA. In conclusion, FSD-prepared balanced steady-state free precession in conjunction with electrocardiography gating and image subtraction provides a promising noncontrast-MRA strategy for the distal lower extremities.

### Keywords

MRI; noncontrast MRA; peripheral arterial disease; PAD; balanced steady-state free precession

---

Peripheral arterial disease (PAD) is a major cause of diminished functional capacity and quality of life in a large portion of western populations and also involved with increased risk of severe cardiovascular events, such as heart attack and stroke (1). While catheter angiography remains the gold standard for the evaluation of vascular disorders (2), MRI has become a routine diagnostic tool in clinical practice because of its noninvasive nature, especially since three-dimensional (3D) contrast-enhanced (CE) magnetic resonance angiography (MRA) has been established to have high diagnostic accuracy for the assessment of peripheral arteries (3–6).

Angiographic imaging of the peripheral vascular tree, particularly in the lower extremities, is challenging due to reduced flow in patients with PAD and uniquely large territories requiring extraordinary fields of view (FOV) or multiple successive scans. Independent of inflow effects, 3D CE-MRA can employ coronal in-plane acquisition, permitting great anatomic coverage

---

\*Correspondence to: Debiao Li, Ph.D., 737 N Michigan Ave, Suite 1600, Chicago, IL 60611. d-li2@northwestern.edu.

within a reasonable scan time. Because of the time constraints imposed by a short contrast arterial-phase window, however, spatial resolution and/or 3D coverage have to be compromised. Venous contamination is often problematic in the calves in clinical lower-extremity MRA examinations when using a three-station bolus-chase protocol, since acquisition of central  $k$ -space at this station may not coincide with the arterial peak of contrast bolus (7). More important, PAD patients are known to be at increased risk of renal disease (8), and potential nephrogenic systemic fibrosis reaction in patients with moderate to severe renal insufficiency caused by gadolinium-based contrast agent mandates referral to other tests (9,10). All limitations above, along with added cost of contrast agent, have triggered a renaissance of interest in noncontrast MRA (NC-MRA).

Conventional NC-MRA techniques, including time-of-flight and phase contrast methods, have failed to gain popularity in clinical practice due to their lengthy acquisition times and possible overestimation of the degree and extent of stenoses resulting from stagnant or turbulent flow-induced dephasing artifacts at or distal to stenoses (7,11).

Flow-independent angiography techniques were previously proposed to exploit the  $T_1$  and  $T_2$  differences to isolate arteries from background tissues and veins (12). Balanced steady-state free precession (bSSFP) is used to acquire flow-independent angiography images because of its high signal-to-noise ratio and time efficiency and flow-independent bright-blood contrast (13–16). A major limitation of this type of method is that the long- $T_2$  tissues, such as deep venous blood, fluid, and edema, are inadequately suppressed by  $T_2$ -preparation and thereby interfere with the visualization of arteries (17).

Electrocardiography (ECG)-triggered fresh blood imaging is a promising NC-MRA technique, which requires acquisition of systolic and diastolic images, followed by image subtraction (18–21). The major advantage of the technique is its independence of inflow of fresh blood into the imaging volume. Therefore, it can be used for imaging arteries with relatively slow flow such as the calf arteries. However, with a relatively long echo train, there is inherent signal loss for the arteries with fast flow and complex flow at and distal to stenoses, which may result in overestimation of stenoses. Moreover, a long echo train may contribute to vessel blurring along the phase-encoding direction owing to  $T_2$  filtration effects.

In this work, we developed a bSSFP-based NC-MRA technique using flow-sensitive dephasing (FSD) magnetization preparation, which causes signal loss for moving spins due to intravoxel dephasing (22,23). Magnitude subtraction of a dark-artery scan acquired with FSD preparation during systole and a bright-artery scan acquired without FSD preparation during mid-diastole results in an artery-only 3D image set. To demonstrate its feasibility, we first started with the distal lower extremity station. Relevant FSD parameters were optimized for excellent MRA image quality on healthy volunteers. Additionally, preliminary results on PAD patients are presented.

## THEORY

A schematic of the proposed NC-MRA technique is shown in Fig. 1. Two ECG-triggered scans are acquired with FSD preparation and  $T_2$  preparation, during systole and diastole, respectively. The dark-artery scan is collected during systole because there is a marked velocity difference between arterial and venous flows and an optimal FSD-preparation can be employed to selectively suppress arterial blood signals while having little effect on venous blood and static tissues. The bright-artery scan is acquired during diastole when arterial flow is substantially slow and thus flow artifacts with bSSFP can be minimized (24). Magnitude subtraction of the two scans allows the visualization of arteries with dramatically suppressed background and venous signals.

## Selective Arterial Flow Suppression and Optimal First-Order Gradient Moment

Phase shifts for moving spins are introduced by the applied field gradients in FSD-preparation. For a single isochromat with a velocity of  $v(\vec{r})$ , phase shift,  $\varphi$ , can be expressed as

$$\varphi = \gamma \cdot v(\vec{r}) \cdot \int G(t) \cdot t \cdot dt = \gamma \cdot v(\vec{r}) \cdot m_1 \quad [1]$$

where  $m_1$  is the first-order gradient moment conveyed by the FSD gradient pulses applied in the direction of  $v(\vec{r})$ . Signal loss due to flow is induced via intravoxel dephasing which, according to Eq. 1, is dependent on velocity profile and  $m_1$ . For a certain velocity profile, the flow suppression capability of FSD-preparation is determined by  $m_1$ .

Haacke et al. (25) presented a mathematical description of the signal loss induced by FSD gradient pulses for a laminar flow model. In a one-dimensional parabolic flow velocity profile, if a pixel is small enough so that the velocity variation within the pixel is approximately linear (Fig. 2a), then the reconstructed signal is given by

$$|\rho| = |\rho_0| \cdot |\text{sinc}(\gamma \alpha m_1 \Delta y / 2)| \quad [2]$$

where  $\rho_0$  is the signal being imaged,  $\gamma$  is gyromagnetic ratio,  $\alpha$  is the slope of velocity variation within the pixel,  $m_1$  is the first-order gradient moment, and  $\Delta y$  is the pixel size. As  $\gamma \alpha m_1 \Delta y / 2 = \pi$  (corresponding to the first zero-crossing point of the sinc function),  $\rho = 0$ , meaning that flow signals are completely eliminated. For laminar flow, the greater the flow velocity, the greater the  $\alpha$ , and  $\gamma \alpha m_1 \Delta y / 2$  approaches  $\pi$  more rapidly.

To suppress venous blood signals in NC-MRA, they need to remain similar between the two scans. Therefore, an optimal  $m_1$  is required to selectively suppress arterial signals while having little effect on venous signals in the FSD-prepared scan. This is made possible because of the large velocity difference between arterial and venous blood flows during systole. Based on the aforementioned model, computer simulations were performed using Mat-lab (The Mathworks, Inc, Natick, MA; version 7.0) for the distal popliteal artery, with parameters empirically chosen as follows: the maximum velocity at systole (i.e., the velocity of axial stream) = 1.2 m/sec, lumen diameter = 4.5 mm, lateral pixel size  $\Delta y = 0.93$  mm, and  $\gamma \alpha m_1 \Delta y / 2 = \pi$ . As shown in Fig. 2b,  $m_1$  of 20–120 mT.ms<sup>2</sup>/m is required to suppress the arterial blood signals across the lumen. These simulation results provide an estimate of the range of  $m_1$  values that may work for imaging lower legs.

### Optimization of the FSD Gradient Waveform

The FSD pulse sequence is a  $90^\circ_x$ - $180^\circ_y$ - $90^\circ_{-x}$  driven equilibrium Fourier transform diffusion preparation module, and identical field gradients are applied symmetrically around the  $180^\circ$  radiofrequency (RF) pulse (26). Our analysis, based on the Bloch equation, reveals that conventional unipolar-gradient pulses (Fig. 3a) in the FSD module can introduce a spatial signal modulation in static tissues, as shown below, if the center  $180^\circ$  RF pulse frequency response is spatially inhomogeneous.

$$M_z = (-\cos\theta \sin^2\varphi + \cos^2\varphi) \cdot M_0 \quad [3]$$

$$\varphi(r) = \gamma \cdot r \cdot A \quad [4]$$

where  $M_z$  is the longitudinal magnetization right after FSD-preparation,  $M_0$  is the equilibrium magnetization,  $\theta$  is the actual flip angle of the  $180^\circ$ -pulse,  $\varphi$  is the phase the static spins accumulate during the FSD gradient before the  $180^\circ$ -pulse, which is dependent on the gradient's net area  $A$ ,  $r$  is the spatial variable along the gradient direction, and  $\gamma$  is the gyromagnetic ratio. The period,  $\lambda$ , of the spatial signal modulation is defined as:

$$\lambda = \frac{\pi}{\gamma \cdot A} \quad [5]$$

A simple solution to circumventing the issue is to have  $\varphi$ , or  $A$ , equal to zero. Therefore, a bipolar-gradient scheme (Fig. 3b) becomes a candidate (27). The two gradient waveforms were tested in this work.

## MATERIALS AND METHODS

Nine healthy subjects (five males and four females, age range = 21–33 years, mean age = 25 years) were studied using the proposed NC-MRA approach, with approval by our institutional review board. In addition, two outpatients (males, 62 and 65 years) referred to clinical CE-MRA for suspected or known PAD were studied. Written informed consent was given by all subjects prior to MRI. Imaging was performed using a 1.5-T clinical whole-body MR system (MAGNETOM Avanto; Siemens AG, Erlangen, Germany). A 16-element peripheral matrix coil positioned anteriorly and laterally, along with a spine coil located posteriorly, was used for signal reception. Subjects were placed feet-first and in a supine position in the scanner.

### Imaging Sequences

In the dark-artery scan, the FSD module was followed by a spectrally selective fat saturation RF module and 10 preparation RF pulses with linearly increasing flip angles before bSSFP data acquisition (Fig. 4a). The FSD gradient pulses were applied in the readout direction only, which coincides with the main blood flow direction. A centric ordering scheme in the phase-encoding direction was used to make best use of the flow-spoiling effects of FSD-preparation, while linear ordering was used in the partition-encoding direction. In the bright-artery scan, the FSD module with the gradient pulses switched off, in effect serving as a  $T_2$  preparation (Fig. 4b), was applied before data acquisition to maintain the same  $T_2$  weighting as in the dark-artery scan for venous blood and static tissues.

### Imaging Protocol

After a triplane scout scan, all subjects underwent a phase contrast flow scan above the popliteal trifurcation. Imaging parameters included encoding velocity = 80 cm/sec, FOV =  $340 \times 138$  mm<sup>2</sup>, acquisition matrix =  $384 \times 156$ , slice thickness = 5.0 mm, 30 cardiac phases, retrospective ECG gating, flip angle =  $30^\circ$ , echo time/pulse repetition time = 2.8/33.3 ms, signal averages = 2, Generalized Autocalibrating Partially Parallel Acquisition (GRAPPA) acceleration factor = 2, acquisition time = 60 heartbeats.

Subsequently, NC-MRA was performed on healthy subjects and patients as follows:

- a. In two healthy subjects, the two FSD gradient waveforms, unipolar and bipolar, were compared. The time point ( $T$ ) of the peak arterial blood flow relative to the R-wave was derived from phase contrast flow data. The dark-artery and bright-artery scans

(starting with FSD- or  $T_2$  preparation) were initiated at arterial “peak-flow” ( $T$ ) and “resting-flow” (mid-diastole), respectively. The unipolar-gradient module used gradient strength  $G$  of 5 mT/m and gradient lobe duration  $\delta$  of 1.1 ms, while the bipolar-gradient module used  $G$  of 5 mT/m and  $\delta$  of 1.2 ms. The first-order gradient moments of the two modules were the same ( $17.4 \text{ mT} \cdot \text{ms}^2/\text{m}$ ), presumably generating identical flow suppression effects.

- b. In each of the nine healthy subjects, a series of FSD gradients with  $G$  ranging from 5 to 25 mT/m in increments of 5 mT/m (corresponding to  $m_1 = 17.4, 34.8, 52.2, 69.6, 87.0 \text{ mT} \cdot \text{ms}^2/\text{m}$ ) and a fixed  $\delta$  of 1.2 ms were employed in the bipolar-gradient module. The order of the gradient strengths was randomized, but for each one, the dark-artery and bright-artery acquisitions were performed in an immediate succession and used for subtraction.
- c. Two patients underwent NC-MRA prior to CE-MRA. The bipolar-gradient FSD module used  $G = 15 \text{ mT/m}$  and  $\delta = 1.2 \text{ ms}$ . CE-MRA of the calves was acquired after pelvis and thigh stations with a bolus-chase approach and injection (0.15 mmol/kg body weight injected at 2 mL/sec followed by 0.075 mmol/kg body weight injected at 0.6 mL/sec) of gadopentetate dimeglumine (Magnevist; Bayer HealthCare Pharmaceuticals Inc., Wayne, NJ) and a 20-mL saline flush (at 2 mL/sec) via an automated injector (Spectris; Medrad, Indianola, PA). A 3D RF-spoiled fast low angle shot sequence was used with the following parameters: echo time/pulse repetition time = 0.9/2.6 ms, flip angle =  $20^\circ$ , receiver bandwidth = 610 Hz/pixel, FOV =  $500 \times 344 \text{ mm}^2$ , acquisition matrix =  $512 \times 211$ , 46 2.0-mm-thick slices (interpolated to 72 1.3-mm-thick slices), GRAPPA acceleration factor = 2.

In all the scans above, bSSFP readout used the same imaging parameters as follows: echo time/pulse repetition time = 1.9/3.8 ms, receiver bandwidth = 965 Hz/pixel, oblique coronal imaging slab with readout in the craniocaudal direction, FOV =  $400 \times 311 \times 67 \text{ mm}^3$  covering major arteries (i.e., the distal popliteal artery, the anterior and posterior tibial arteries, and the peroneal artery) in both lower legs, acquisition matrix =  $432 \times 336 \times 72$  leading to an isotropic resolution of  $0.9 \times 0.9 \times 0.9 \text{ mm}^3$ , flip angle =  $90^\circ$ , three shots per partition (60 lines per cardiac cycle), GRAPPA acceleration factor = 2 in the phase-encoding direction, acquisition time = 3 – 4 min per scan.

## Image Analysis

All 3D data sets were processed and evaluated on a workstation (Leonardo; Siemens AG).

In assessing the images acquired in protocol (a), the paired bright-artery and dark-artery images underwent magnitude subtraction, and maximum intensity projection (MIP) images of the subtracted data sets were created for image quality evaluation via visual inspection.

The NC-MRA images acquired in protocol (b) underwent qualitative assessment to reveal the effects of  $m_1$ . Measurements of signal-to-noise ratio and contrast-to-noise ratio were not performed because of the inhomogeneous spatial distribution of noise in images acquired with parallel imaging. Five subtraction MRA MIP images corresponding to various FSD gradient strengths were created for each subject. Two experienced radiologists (J.C. and J.S.), blinded to subject identity, as well as FSD gradient strengths, reviewed all source and subtracted 3D data sets, as well as MIP images, for image quality in a random order. In each leg, the artery territory was divided into three portions in the craniocaudal direction. A consensus score was given to each portion on a four-point scale: 1, nondiagnostic due to poor delineation of major arteries or severe venous contamination; 2, fair delineation of major arteries or some venous contamination; 3, good delineation of major arteries or minor venous contamination; 4,

excellent delineation of major arteries and no venous contamination. One score was obtained for each leg by averaging the three scores from individual portions.

Finally, the NC-MRA and CE-MRA data sets from patients (protocol (c)) were reviewed by the two radiologists in consensus to qualitatively assess the diagnostic ability of the NC-MRA technique.

### Statistical Analysis

The image scores obtained from the five FSD gradient strengths in protocol (b) were analyzed statistically. Data were presented as means  $\pm$  standard deviations. In each subject, average image score was calculated, and statistical analyses were on a per-subject basis. A Friedman test was used to determine whether image score varies with the FSD gradient strength. Furthermore, Wilcoxon signed rank tests were performed to compare the highest image score to those from other gradient strengths. In all tests, statistical significance was defined at  $P < 0.05$ . SPSS version 16.0 (Chicago, IL) was used for all statistical analyses.

## RESULTS

Figure 5 illustrates how the NC-MRA technique worked on a healthy subject. In the bright-artery scan (Fig. 5a,d), both arterial and venous lumens appeared bright. Arterial blood signals were dramatically eliminated in the dark-artery scan (Fig. 5b,e), whereas venous blood and other static tissues were barely affected by the FSD-preparation with  $m_1$  of  $34.8 \text{ mT} \cdot \text{ms}^2/\text{m}$ . Hence, major branches of the calf arteries were exclusively highlighted upon image subtraction (Fig. 5c,f).

In the two subjects, the images acquired using the unipolar-gradient FSD module showed appreciable stripe artifacts, some of which interfered with the artery visualization on subtraction MIPs (Fig. 6a). However, these artifacts disappeared when using the bipolar-gradient FSD module (Fig. 6b).

Figure 7 shows the representative coronal subtraction MIP images from one healthy subject, obtained using bipolar-gradient FSD-prepared bSSFP. At low FSD gradient strengths, major branches of the calf arteries were clearly depicted. As the gradient strength increased from 5 to 25 mT/m, more and more sub-branches of the arteries became visible. Meanwhile, more veins also appeared and contaminated artery delineation. The gradient of  $G = 10 \text{ mT/m}$  was found to consistently offer excellent delineation of arteries and contrast between arteries and background, including static tissues and veins.

Qualitative assessment is illustrated in Fig. 8. Within the range of FSD gradient strengths tested, image quality was significantly affected by gradient strength ( $P = 0.003$ ). The image scores from the gradient of  $G = 10 \text{ mT/m}$  ( $3.8 \pm 0.3$ ) were significantly higher than those from  $G = 15$  ( $3.5 \pm 0.3$ ;  $P = 0.018$ ), 20 ( $3.2 \pm 0.5$ ;  $P = 0.011$ ), and 25 mT/m ( $3.4 \pm 0.6$ ;  $P = 0.028$ ), and very close to but still higher than that from  $G = 5 \text{ mT/m}$  ( $3.7 \pm 0.4$ ).

In the two patients, NC-MRA provided excellent MRA images, with sharper artery delineation due to higher and isotropic spatial resolution in comparison to CE-MRA. In one patient, a mild stenosis at the origin of the right peroneal artery was identified by NC-MRA, which was confirmed by CE-MRA (Fig. 9); however, a narrowing at the origin of the right posterior tibial artery was only shown on the NC-MRA image. In another patient, both CE-MRA and NC-MRA demonstrated significant bilateral calf artery occlusion (Fig. 10). The large collateral vessels were not well depicted on the CE-MRA image owing to incomplete enhancement (right leg) or venous overlay (left leg). On the other hand, the patent bypass graft of the left leg shown

on the CE-MRA image appeared to have a stenosis on the NC-MRA image, which is most likely due to the adjacent metallic clip-induced signal loss in the bright-artery scan (Fig. 10c).

## DISCUSSION

In this work, a 3D NC-MRA technique based on segmented bSSFP combing ECG-triggering, FSD magnetization preparation, and subtraction techniques was developed and tested on the calf arteries. 3D isotropic submillimeter-spatial-resolution angiograms with bright arterial blood and dramatically suppressed background were successively obtained in all healthy volunteers and patients.

FSD preparation was used to induce arterial flow voids at systolic cardiac phase while having little effect on venous blood and static tissues. The  $m_1$  conveyed by FSD preparation is the key to blood signal suppression. Optimization of  $m_1$  was explored on healthy volunteers in this work, giving rise to two findings. First, this procedure revealed the determinant role of  $m_1$  in suppressing the blood signals and achieving excellent MRA quality. As estimated by computer simulations,  $m_1$  of at least  $20\text{--}120\text{ mT} \cdot \text{ms}^2/\text{m}$  is required to suppress arterial blood signals if the flowing spins' velocity varies along a single direction. With generalization of the one-dimensional to the two-dimensional velocity profile in which velocity varies within the entire cross-section, the value of  $m_1$  for sufficient blood suppression would be anticipated to be even lower. Qualitative image evaluation has shown that all gradient strengths tested herein were able to produce an MRA image with at least good image quality (image quality score of 3). Their corresponding  $m_1$ 's were within the range of  $17\text{--}87\text{ mT} \cdot \text{ms}^2/\text{m}$ , which accords with the simulation results. Second, an optimal  $m_1$  value for lower-extremity MRA was identified for healthy volunteers, which may aid in a screening test of distal lower-extremity vascular disease. In this work,  $m_1$  of  $34.8\text{ mT} \cdot \text{ms}^2/\text{m}$  (i.e.,  $G = 10\text{ mT/m}$ ) was shown to generate superior image quality. The lower image scores when using higher  $m_1$ 's primarily resulted from venous contamination as induced by partial venous signal suppression in the dark-artery scan. Additionally,  $m_1$  of lower than  $34.8\text{ mT} \cdot \text{ms}^2/\text{m}$  also showed impaired image quality, most likely owing to the weak suppression of the arterial signals. Since FSD gradient optimization was not performed in patients, inadequate  $m_1$  and thus insufficient blood suppression in the dark-artery scan were thought to contribute in part to vessel narrowing (Fig. 9b).

Because of FSD's sensitivity to flow velocity, ECG triggering was shown to help FSD eliminate arterial blood signals. Specifically, when arterial flow reaches its peak in every cardiac cycle, small FSD gradient pulses are capable of suppressing arterial signals without substantially affecting venous flow. At other cardiac phases, FSD pulses have to be accordingly enhanced to achieve satisfactory blood suppression, and side effects, however, would be more suppression of venous blood signals.

In this study, stripe artifacts were observed in the unipolar-gradient FSD scan. It is therefore inferred that the flip angle of the center  $180^\circ$ -pulse was not essentially  $180^\circ$  due to amplitude of RF field inhomogeneity, which may get worse when a hard RF pulse is used for a large-FOV imaging. In our preliminary work, it has been found that the artifacts became more pronounced as gradient strength, if duration is held fixed, was reduced. Clearly, this is explained by reduced  $A$  and therefore increased  $\lambda$  in Eq. 5. Although the artifacts resided in static tissues, the visualization of arteries was always compromised, especially on MIP images. The bipolar-gradient FSD scheme provides a solution by letting  $A$  equal 0. Hence Eq. 3 reduces to  $M_z = M_0$ , leading to no spatial modulation of signals in the presence of inhomogeneous amplitude of RF field.

Additional effects of the FSD preparation on static spins involve signal loss caused by diffusion and  $T_2$  decay. The former issue can almost be ignored because of very little diffusion  $b$  value

(e.g.,  $b = 0.02 \text{ sec/mm}^2$  when  $m_1 = 34.8 \text{ mT} \cdot \text{ms}^2/\text{min}$  the bipolar-gradient FSD module). This has been reflected by the satisfactorily clean background on the subtracted images in the present work. The latter issue was alleviated by using a short-duration FSD module with only 9-msec  $T_2$  decay. In addition, FSD and  $T_2$  preparation with the same duration were used in dark-artery and bright-artery scans, respectively, and surrounding tissues would be mostly eliminated upon subtraction due to the same  $T_2$  decay in both scans.

A few of strengths of the FSD-prepared bSSFP technique can be accentuated by comparing it with other conventional, as well as newly developed, NC-MRA methods. MRA depicts the arterial tree by highlighting blood flow rather than blood vessel itself. Any flow-void effects may lead to overestimation of lumen stenoses (28). This is a problem usually occurring in time-of-flight and phase contrast MRA because the flow at or distal to arterial stenoses is slow or turbulent, especially near the lumen edge. Theoretically speaking, however, the presented flow-spoiled MRA technique is advantageous in near-edge flow due to locally large velocity variation and thus adequate phase dispersion (Fig. 2). Turbulent flow can also be readily suppressed with FSD sensitivity configured in multiple directions. On the other hand, in the presence of stagnant flow, the new technique could become effective by strengthening the FSD's  $m_1$ , likely at the cost of simultaneous venous flow suppression. These potential benefits and issues await a systematic comparison in a future clinical study.

The FSD-prepared NC-MRA method is flow dependent but does not rely on inflow of blood into the imaging volume. Although various inflow-based methods have recently showed promising results, depiction of arteries may likely be impaired due to incomplete inflow/outflow of fresh or prelabled blood spins into the imaging volume (29,30). The use of FSD preparation may enable a flexible imaging orientation and great anatomic coverage without this issue. This is analogous to the flow-independent angiography methods by Brittain et al. (12), but the FSD-prepared method can reliably offer angiogram with substantially darker background through image subtraction.

In contrast to the fresh blood imaging technique where 3D turbo spin + echo (TSE) combined with flow-spoiling gradients is used, our technique employs bSSFP acquisition in conjunction with an independent flow-suppression preparation module. As with fresh blood imaging, the new approach was demonstrated with blood suppression exerted in the readout direction only, potentially rendering suboptimal suppression in some arterial branches or bifurcations that contain flow in a different direction from the craniocaudal direction (Fig. 9). Admittedly, this is a limitation in the present study. However, in theory, the FSD gradient pulses can be flexibly configured in both direction and strength, and therefore multidirectional flow suppression is feasible with a sophisticated pulse configuration. However, this flexibility is not inherent to the fresh blood imaging sequence. In addition, due to the separation between flow suppression and data acquisition, the dark-blood contrast in the dark-artery scan is exclusively determined by the FSD module, and the flow-suppression effect can be easily quantified and predicted by calculating the first-order gradient moment in the FSD module. Finally, compared to TSE, bSSFP itself is better suited for bright-blood imaging of fast flow, as well as avoiding  $T_2$ -decay-induced vessel blurring, owing to its balanced gradient structure. A variant of the 3D TSE, has been recently proposed to alleviate the  $T_2$  filtration effects by shortening the acquisition window and acquiring signal in a pseudosteady state by virtue of nonselective variable-flip-angle refocusing RF pulses (31). Whether the gradient-echo technique outperforms the spin-echo technique in terms of flow suppression and vessel sharpness would be a future research subject of interest.

The proposed NC-MRA technique was successively demonstrated at 1.5 T. Imaging at higher field strength, such as 3 T, will favor the blood signal-to-noise ratio and blood-tissue contrast-to-noise ratio, which can in turn be traded for higher spatial resolution or a reduced imaging

time. However, bSSFP images at 3 T may be degraded by pronounced off-resonance artifacts arising from increased susceptibility effects. This issue could be exacerbated in peripheral MRA, given that a large field of view is needed. Previous studies have investigated the feasibility of bSSFP at 3 T for noncontrast lower-extremity MRA and presented promising results (13,15). Thus, the FSD-prepared MRA technique could be applicable at 3 T upon a specialized optimization of relevant imaging parameters.

The new technique does have several drawbacks with respect to its design. First, it requires long imaging time due to ECG-triggering and image subtraction, making it more prone to motion-induced image blurring, as well as image-distorting motion artifacts. Some postprocessing motion correction approaches may help minimize the latter issue, such as breast acquisition and correction (BRACE; Siemens; software for 3D nonrigid registration), available on Siemens systems (32). Also, interleaving the bright-artery scan with dark-artery scan would be able to reduce misregistration artifacts. An acceleration factor of 2 (GRAPPA) has been used in this study and artery signals appeared sufficiently high. Considering the high signal-to-noise ratio efficiency of bSSFP, there is still room to increase parallel imaging acceleration factor to 3 or even higher. Second, the bright-artery scan and dark-artery scan need to be triggered at different cardiac phases, and pulsatile vessel diameter change may influence arterial depiction, although it could be neglected in small-caliber arteries (e.g., vary by 0.19 mm in the femoral artery) when using a 0.9-mm spatial resolution (33). The bright-artery images are not acquired during systole owing to inadequate flow compensation in bSSFP sequence when using nonlinear view-ordering schemes (34). The linear centric-encoding concept and/or addition of flow-compensating gradient waveform into each pulse repetition time cycle in all three directions can be remedies to this issue (34,35). It is desirable that both scans be conducted at the systolic cardiac phase. Third, an approach to identify optimal  $m_1$  that would vary with patient and disease is not yet developed. Obviously, it is time consuming if optimization procedure described in this work is conducted for each patient. A fast  $m_1$  scouting approach may help improve the robustness and efficiency of this technique.

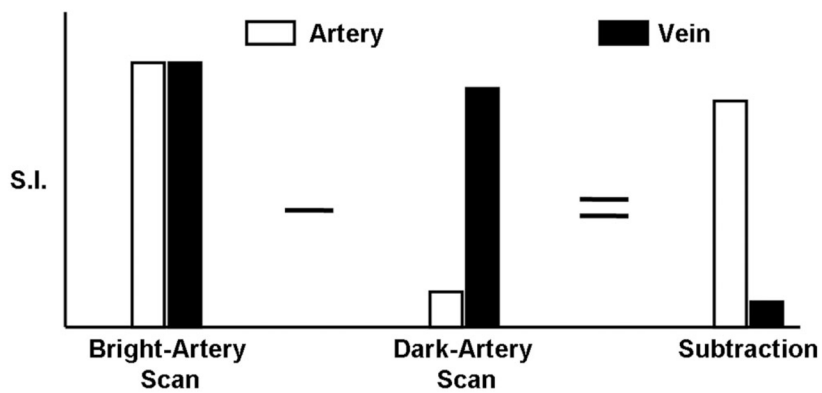
In conclusion, a subtraction-based NC-MRA technique using ECG-triggered 3D segmented bSSFP with FSD preparation has been developed and validated in the distal lower extremities of healthy volunteers. It allows for artery visualization with high isotropic spatial resolution, large FOV, and excellent contrast between arteries and surrounding veins and tissues without the use of contrast agent. With the flexibility of choice on FSD gradient strength and direction, this technique may be easily accommodated to individual physiologic conditions of PAD patients and have the potential for MRA of other vascular territories. In particular, it is of great interest to explore its applicability in the abdominopelvis and thighs, thus achieving entire lower extremity MRA. Nevertheless, this technique merits further technical improvements and systematic clinical studies to clarify its diagnostic ability.

## References

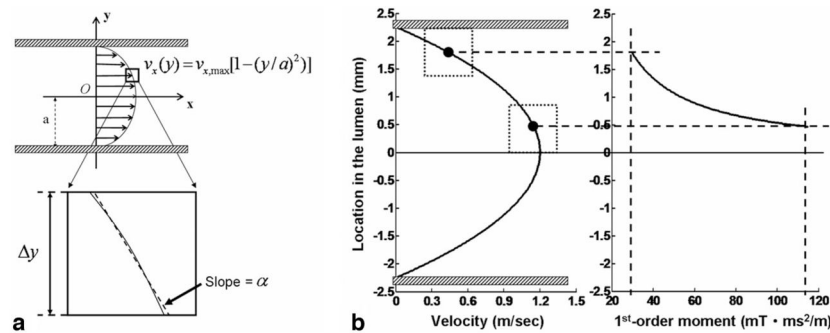
1. Pasternak RC, Criqui MH, Benjamin EJ, Fowkes FG, Isselbacher EM, McCullough PA, Wolf PA, Zheng ZJ. Atherosclerotic Vascular Disease Conference: Writing Group I: epidemiology. *Circulation* 2004;109:2605–2612. [PubMed: 15173042]
2. Borrello JA. MR angiography versus conventional X-ray angiography in the lower extremities: everyone wins. *Radiology* 1993;187:615–617. [PubMed: 8497604]
3. Ruehm SG, Hany TF, Pfammatter T, Schneider E, Ladd M, Debatin JF. Pelvic and lower extremity arterial imaging: diagnostic performance of three-dimensional contrast-enhanced MR angiography. *Am J Roentgenol* 2000;174:1127–1135. [PubMed: 10749264]
4. Loewe C, Schoder M, Rand T, Hoffmann U, Sailer J, Kos T, Lammer J, Thurnher S. Peripheral vascular occlusive disease: evaluation with contrast-enhanced moving-bed MR angiography versus digital subtraction angiography in 106 patients. *Am J Roentgenol* 2002;179:1013–1021. [PubMed: 12239057]

5. Deutschmann HA, Schoellnast H, Portugaller HR, Preidler KW, Reittner P, Tillich M, Pilger E, Szolar DH. Routine use of three-dimensional contrast-enhanced moving-table MR angiography in patients with peripheral arterial occlusive disease: comparison with selective digital subtraction angiography. *Cardiovasc Intervent Radiol* 2006;29:762–770. [PubMed: 16625410]
6. Ersoy H, Rybicki FJ. MR angiography of the lower extremities. *AJR Am J Roentgenol* 2008;190:1675–1684. [PubMed: 18492924]
7. Meaney JF, Sheehy N. MR angiography of the peripheral arteries. *Magn Reson Imaging Clin N Am* 2005;13:91–111. vi. [PubMed: 15760758]
8. O'Hare AM, Bertenthal D, Shlipak MG, Sen S, Chren MM. Impact of renal insufficiency on mortality in advanced lower extremity peripheral arterial disease. *J Am Soc Nephrol* 2005;16:514–519. [PubMed: 15601746]
9. Grobner T. Gadolinium: a specific trigger for the development of nephrogenic fibrosing dermopathy and nephrogenic systemic fibrosis? *Nephrol Dial Transplant* 2006;21:1104–1108. [PubMed: 16431890]
10. Marckmann P, Skov L, Rossen K, Dupont A, Damholt MB, Heaf JG, Thomsen HS. Nephrogenic systemic fibrosis: suspected causative role of gadodiamide used for contrast-enhanced magnetic resonance imaging. *J Am Soc Nephrol* 2006;17:2359–2362. [PubMed: 16885403]
11. Miyazaki M, Lee VS. Nonenhanced MR angiography. *Radiology* 2008;248:20–43. [PubMed: 18566168]
12. Brittain JH, Olcott EW, Szuba A, Gold GE, Wright GA, Irrarrazaval P, Nishimura DG. Three-dimensional flow-independent peripheral angiography. *Magn Reson Med* 1997;38:343–354. [PubMed: 9339435]
13. Brittain, JH.; Shimakawa, A.; Wright, GA.; Hargreaves, BA.; Han, E.; Stainsby, JA.; Hu, B. Non-contrast-enhanced, flow-independent, 3D peripheral angiography using steady-state free precession at 3T. Proceedings of the 11th Annual Meeting of ISMRM; Toronto, Ontario, Canada. 2003. p. 1710
14. Bangerter, NK.; Hargreaves, BA.; Brittain, JH.; Hu, B.; Vasawala, SS.; Nishimura, DG. 3D fluid-suppressed T2-prep flow-independent angiography using balanced SSFP. Proceedings of the 12th Annual Meeting of ISMRM; Kyoto, Japan. 2004. p. 11
15. Stafford RB, Sabati M, Mahallati H, Frayne R. 3D non-contrast-enhanced MR angiography with balanced steady-state free precession Dixon method. *Magn Reson Med* 2008;59:430–433. [PubMed: 18183607]
16. Scheffler K, Lehnhardt S. Principles and applications of balanced SSFP techniques. *Eur Radiol* 2003;13:2409–2418. [PubMed: 12928954]
17. Gronas R, Kalman PG, Kucey DS, Wright GA. Flow-independent angiography for peripheral vascular disease: initial in-vivo results. *J Magn Reson Imaging* 1997;7:637–643. [PubMed: 9243381]
18. Wedeen VJ, Meuli RA, Edelman RR, Geller SC, Frank LR, Brady TJ, Rosen BR. Projective imaging of pulsatile flow with magnetic resonance. *Science* 1985;230:946–948. [PubMed: 4059917]
19. Miyazaki M, Sugiura S, Tateishi F, Wada H, Kassai Y, Abe H. Non-contrast-enhanced MR angiography using 3D ECG-synchronized half-Fourier fast spin echo. *J Magn Reson Imaging* 2000;12:776–783. [PubMed: 11050650]
20. Miyazaki M, Takai H, Sugiura S, Wada H, Kuwahara R, Urata J. Peripheral MR angiography: separation of arteries from veins with flow-spoiled gradient pulses in electrocardiography-triggered three-dimensional half-Fourier fast spin-echo imaging. *Radiology* 2003;227:890–896. [PubMed: 12702824]
21. Lim RP, Hecht EM, Xu J, Babb JS, Oesingmann N, Wong S, Muhs BE, Gagne P, Lee VS. 3D nongadolinium-enhanced ECG-gated MRA of the distal lower extremities: preliminary clinical experience. *J Magn Reson Imaging* 2008;28:181–189. [PubMed: 18581339]
22. Sirol M, Itskovich VV, Mani V, Aguinaldo JG, Fallon JT, Misselwitz B, Weinmann HJ, Fuster V, Toussaint JF, Fayad ZA. Lipid-rich atherosclerotic plaques detected by gadofluorine-enhanced in vivo magnetic resonance imaging. *Circulation* 2004;109:2890–2896. [PubMed: 15184290]
23. Koktzoglou I, Li D. Diffusion-prepared segmented steady-state free precession: application to 3D black-blood cardiovascular magnetic resonance of the thoracic aorta and carotid artery walls. *J Cardiovasc Magn Reson* 2007;9:33–42. [PubMed: 17178678]

24. Markl M, Alley MT, Elkins CJ, Pelc NJ. Flow effects in balanced steady state free precession imaging. *Magn Reson Med* 2003;50:892–903. [PubMed: 14586999]
25. Haacke, EM.; Brown, RW.; Thompson, MR.; Venkatesan, R. *Magnetic resonance imaging physical principles and sequence design*. Vol. 23. New York: Wiley-Liss; 1999. p. 673-675.
26. Becker ED, Farrar TC. Driven equilibrium Fourier transform spectroscopy: a new method for nuclear magnetic resonance signal enhancement. *J Am Chem Soc* 1969;91:7784–7785. [PubMed: 5357869]
27. Nguyen TD, de Rochefort L, Spincemaille P, Cham MD, Weinsaft JW, Prince MR, Wang Y. Effective motion-sensitizing magnetization preparation for black blood magnetic resonance imaging of the heart. *J Magn Reson Imaging* 2008;28:1092–1100. [PubMed: 18972350]
28. Urchuk SN, Plewes DB. Mechanisms of flow-induced signal loss in MR angiography. *J Magn Reson Imaging* 1992;2:453–462. [PubMed: 1633399]
29. Liu X, Berg N, Sheehan J, Bi X, Weale P, Jerecic R, Carr J. Renal transplant: nonenhanced renal MR angiography with magnetization-prepared steady-state free precession. *Radiology* 2009;251:535–542. [PubMed: 19261926]
30. Koktzoglou I, Edelman RR. STAR and STARFIRE for flow-dependent and flow-independent noncontrast carotid angiography. *Magn Reson Med* 2009;61:117–124. [PubMed: 19097217]
31. Xu, J.; Weale, P.; Gerhard, L.; Schmitt, P.; Park, J.; Stoeckel, B.; Chen, Q.; Lim, RP.; Hardie, A.; Storey, P.; Hecht, EM.; MCGorty, K.; Lee, VS. A novel non-contrast MR angiography technique using triggered non-selective refocused SPACE for improved spatial resolution and speed. *Proceedings of the 16th Annual Meeting of ISMRM; Toronto, Ontario, Canada. 2008. p. 730*
32. Herrmann KH, Wurdinger S, Fischer DR, Krumbein I, Schmitt M, Hermosillo G, Chaudhuri K, Krishnan A, Salganicoff M, Kaiser WA, Reichenbach JR. Application and assessment of a robust elastic motion correction algorithm to dynamic MRI. *Eur Radiol* 2007;17:259–264. [PubMed: 16612550]
33. Eriksen M. Effect of pulsatile arterial diameter variations on blood flow estimated by Doppler ultrasound. *Med Biol Eng Comput* 1992;30:46–50. [PubMed: 1640754]
34. Bieri O, Scheffler K. Flow compensation in balanced SSFP sequences. *Magn Reson Med* 2005;54:901–907. [PubMed: 16142709]
35. Bi X, Park J, Deshpande V, Simonetti O, Laub G, Li D. Reduction of flow- and eddy-currents-induced image artifacts in coronary magnetic resonance angiography using a linear centric-encoding SSFP sequence. *Magn Reson Imaging* 2007;25:1138–1147. [PubMed: 17905246]

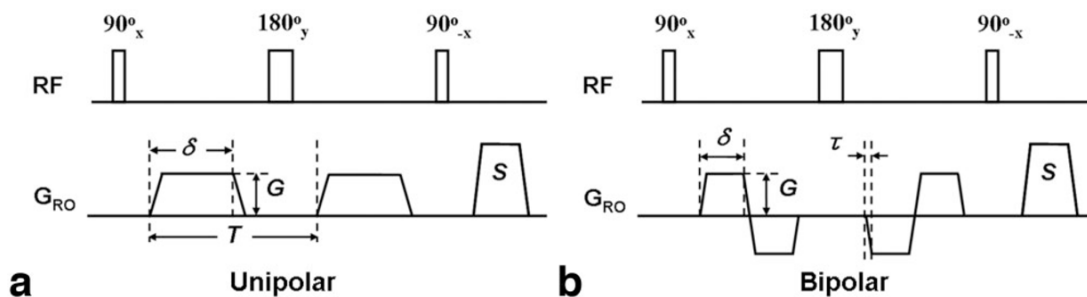


**FIG. 1.** Schematic of the FSD-prepared NC-MRA technique. In the bright-artery scan, both arterial blood and venous blood are of high signal intensity. In the dark-artery scan, arterial blood signals are mostly suppressed by FSD-preparation, whereas venous blood signals are only slightly reduced because of substantially slow flow. Thus, arterial blood signals remain and venous blood signals almost disappear upon image subtraction.



**FIG. 2.**

**a:** A one-dimensional laminar flow velocity profile is described by a parabolic equation as shown in the figure, and if the pixel is small enough, the profile within the pixel is approximately linear with a slope of  $\alpha$ . **b:** Computer simulations based on the one-dimensional flow model reveal a range of the first-order gradient moment ( $\alpha$ ) capable of suppressing the arterial blood flow. Greater  $m_1$  is required to suppress the flow signals when the pixel of interest transits from the lumen edge to the lumen center. The two solid dots in **(b)** represent the centers of the two pixels with their boundaries (dotted lines) located at the lumen edge and the lumen center, respectively. The parameters used in simulations include the maximum velocity  $v_{\max} = 1.2$  m/sec, lumen diameter  $2a = 4.5$  mm, pixel size  $\Delta y = 0.93$  mm, and  $\gamma \alpha m_1 \Delta y / 2 = \pi$ . ( $\gamma$  is gyromagnetic ratio).

**FIG. 3.**

Diagrams of the unipolar- **(a)** and bipolar-gradient **(b)** FSD modules. Both modules consist of a  $90^\circ_x$ - $180^\circ_y$ - $90^\circ_{-x}$  RF series and two symmetric FSD gradient pulses placed at either side of the center  $180^\circ$ -pulse. The FSD gradient pulses can be applied in the any of the three directions, for example, the readout direction ( $G_{RO}$ ).  $G$ : gradient strength;  $\delta$ : gradient duration;  $\tau$ : gradient ramp-up time;  $S$ : spoiling gradients to destroy remnant transverse magnetization;  $T$ : interval between the two unipolar gradient pulses.  $G$  and  $\delta$  are specifiable through the user interface, depending on how strong a first-order gradient moment is needed. Other parameters are held fixed as follows:  $90^\circ$  pulse and  $180^\circ$  pulse have durations of 0.5 ms and 1 ms, respectively,  $\tau = 0.25$  ms.

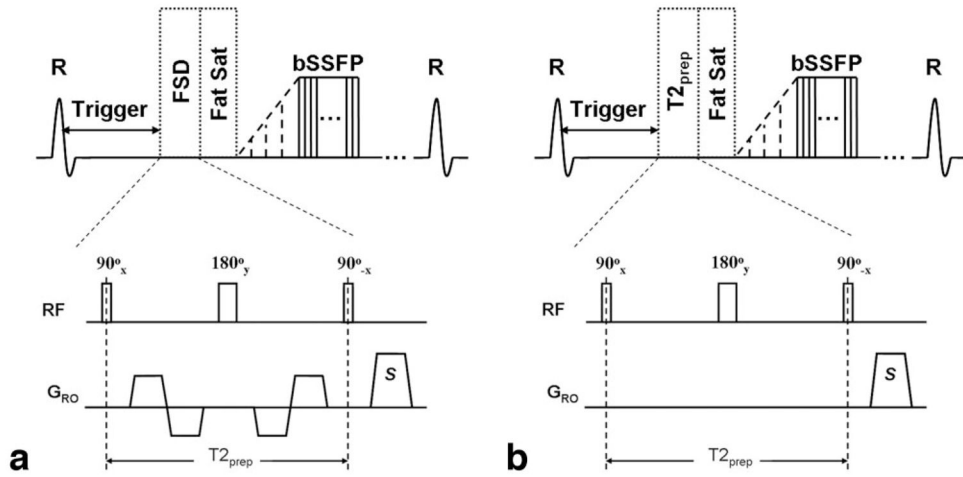


**FIG. 4.**

Sequence diagram of the dark-artery scan using FSD-prepared bSSFP triggered at systole **(a)** and the bright-artery scan using  $T_2$ -prepared bSSFP triggered at diastole **(b)**. Both FSD preparation and  $T_2$  preparation consist of a  $90^\circ_x$ - $180^\circ_y$ - $90^\circ_x$  RF series and are of the same duration (i.e.,  $T_{2\text{prep}}$ ) to maintain the same  $T_2$  weighting for venous blood and static tissues. The FSD gradient pulses applied in the readout direction ( $G_{RO}$ ) only are switched on in FSD-preparation but switched off in  $T_2$  preparation. The readout direction coincides with the main blood flow direction. FSD or  $T_2$  preparation is followed by a spectrally selective fat saturation RF module and 10 preparation RF pulses with linearly increasing flip angles prior to bSSFP data acquisition.

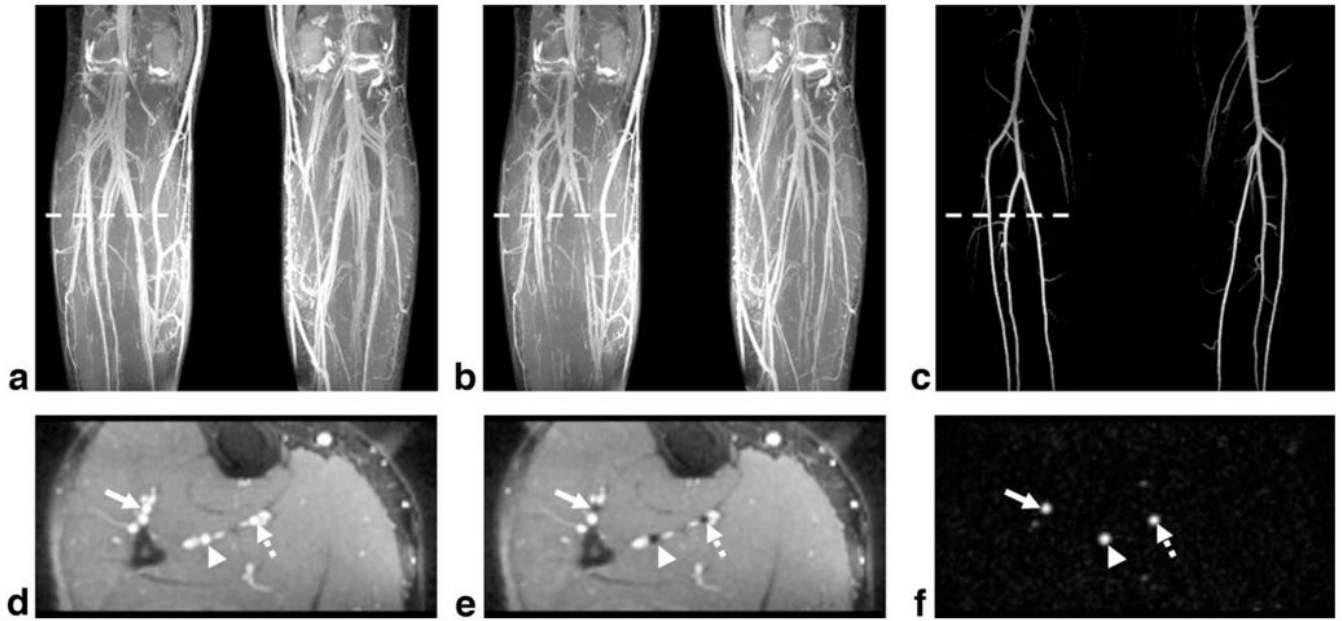
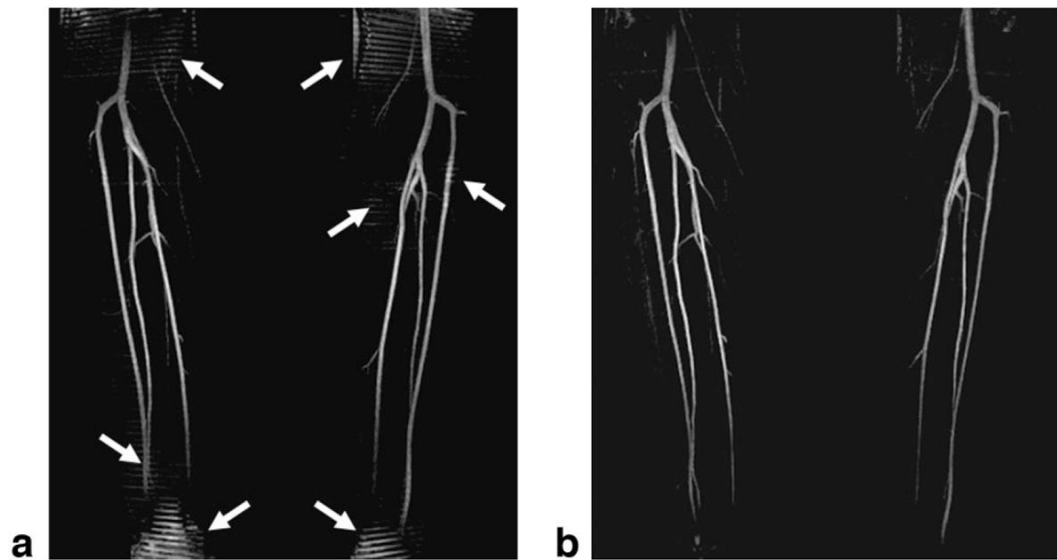
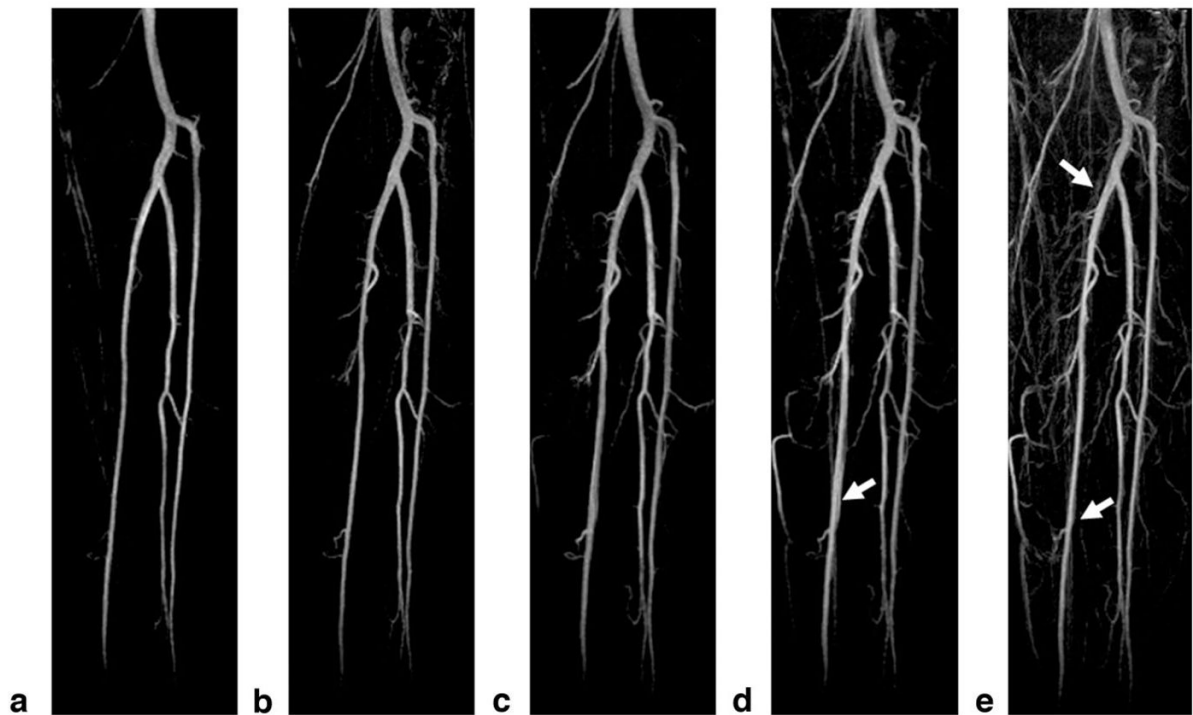
**FIG. 5.**

Image demonstration of the subtraction-based NC-MRA technique. **a–c**: Coronal MIPs created from the 3D data sets obtained in the bright-artery scan, dark-artery scan, and subtraction, respectively. **d–f**: The transverse images reformatted from the same locations (marked as the dashed lines in **a–c**) in the 3D data sets used for creating **(a–c)**. Both the arteries and veins are depicted as bright blood in the bright-artery scan (**a,d**). However, the signals in the major branches of the calf arteries (arrow: the anterior tibial artery; arrowhead: the peroneal artery; dashed arrow: the posterior tibial artery) are dramatically suppressed by FSD preparation, which has little effect on the veins and static tissues (**b,e**). The resultant subtraction images (**c,f**) show excellent artery delineation and dramatically clean background. In this case, FSD preparation used a bipolar-gradient waveform with gradient strength of 10 mT/m and duration of 1.2 ms.



**FIG. 6.** Subtraction MIP images obtained using the unipolar- (a) and bipolar-gradient FSD module (b), respectively. Both FSD modules achieve a similar flow suppression due to the same first-order gradient moments ( $17.4 \text{ mT} \cdot \text{ms}^2/\text{m}$ ). However, the stripe artifacts shown on the unipolar-gradient FSD images interfere with the visualization of main arterial branches to some degree (arrows), which are removed by the bipolar-gradient FSD module.

**FIG. 7.**

Representative subtraction MIP images from a healthy subject obtained using the proposed NC-MRA technique with the FSD gradient duration  $\delta = 1.2$  ms and strength  $G = 5$  mT/m (a), 10 mT/m (b), 15 mT/m (c), 20 mT/m (d), and 25 mT/m (e), respectively. At low FSD gradient strengths, major branches of the calf arteries are well depicted, with sufficiently clean background. As the FSD gradient strength increases from 5 to 25 mT/m, more and more sub-branches of the arteries become visible, and on the other hand, more veins and background signals also appear, contaminating artery delineation on MIPs (arrows). All images are displayed with the same window level.

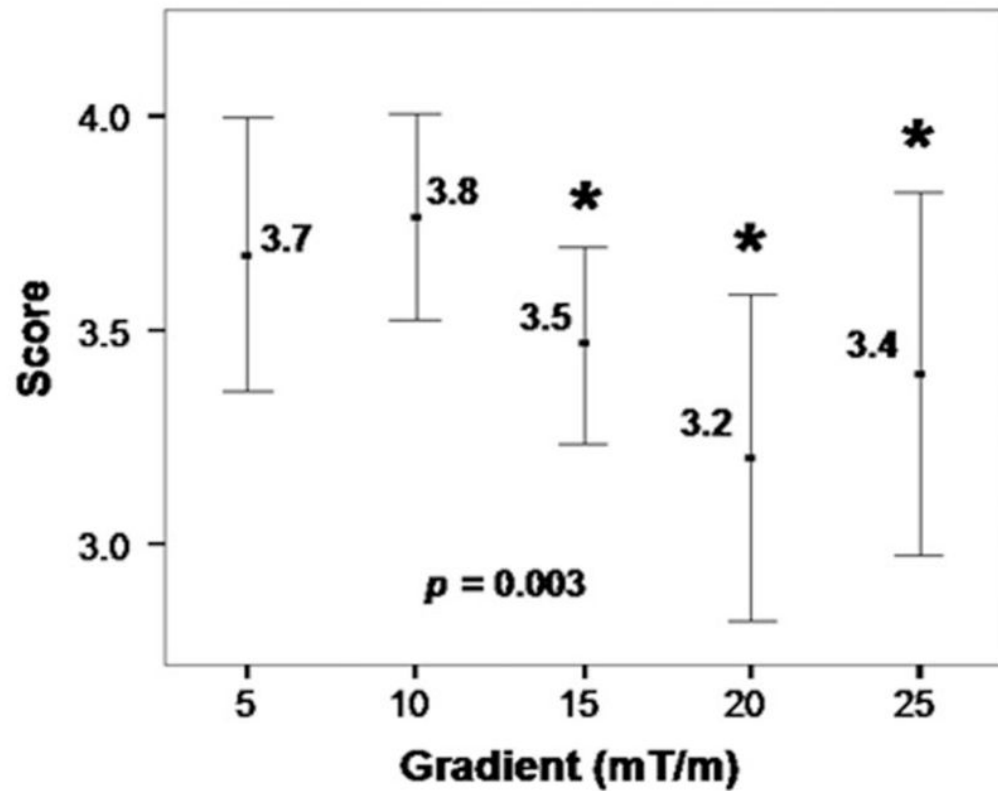


**FIG. 8.**

The dependence of image quality score on FSD gradient strength derived from healthy volunteer studies ( $n = 9$ ). FSD gradient strength has a significant effect on image quality score ( $P = 0.003$ ) according to a Friedman test. All five gradient strengths are able to generate MRA images with satisfactory diagnostic quality (at least 3 on a 4-point scale). The gradient strength of 10 mT/m results in the highest image scores, which are significantly higher than those from some of the other groups (indicated by \*) according to Wilcoxon signed rank tests. Error bars show 95.0% confidence interval of mean value.

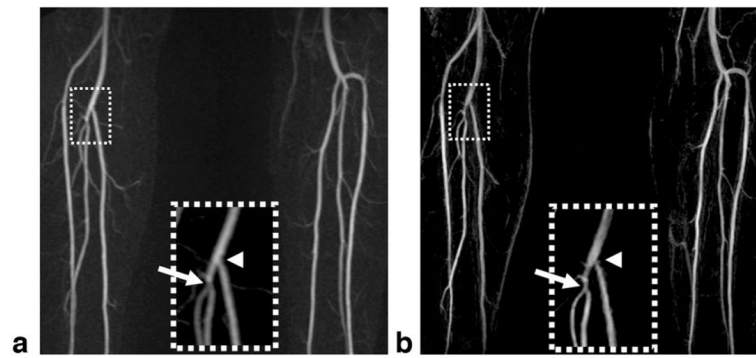


**FIG. 9.** Subtraction MIP images for CE-MRA (a) and NC-MRA (b) in a 62-year-old male patient presenting with right leg claudication. Both techniques detect a mild stenosis at the origin of the right peroneal artery (arrow). However, a narrowing at the origin of the right posterior tibial artery (arrowhead) is only shown on the NC-MRA image. Inspection of the source images confirms that the narrowing is caused by suboptimal blood suppression in the dark-artery scan. Note that NC-MRA demonstrates sharper artery delineation due to higher and isotropic spatial resolution ( $0.9 \times 0.9 \times 0.9 \text{ mm}^3$  vs  $1.0 \times 1.6 \times 1.3 \text{ mm}^3$  (after interpolation)).

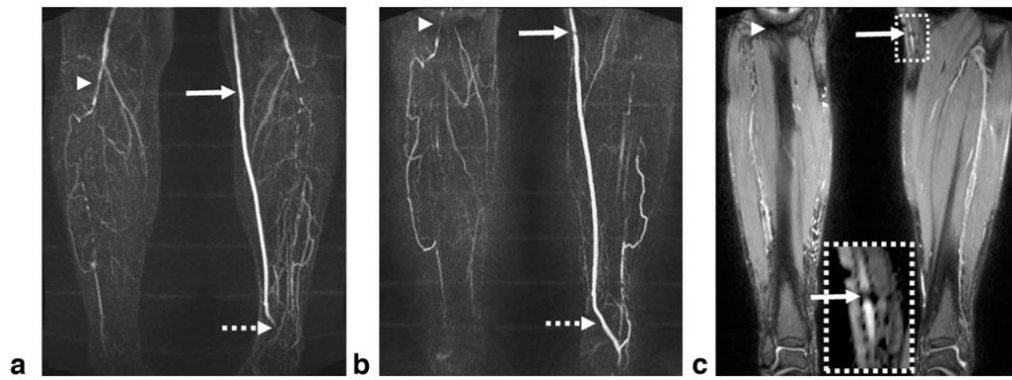


**FIG. 10.** Subtraction MIP images for CE-MRA (**a**) and NC-MRA (**b**) in a 65-year-old male patient with known PAD. Both techniques demonstrate significant bilateral calf artery occlusion. The large collateral vessels are not well delineated on the CE-MRA image due to incomplete arterial enhancement (right leg) or venous overlay (left leg). The patent bypass graft (CE-MRA image) appears to have a stenosis (solid arrow) on the NC-MRA image, which is most likely due to the adjacent metallic clip–induced signal loss in the bright-artery scan (**c**). The distal part of the bypass graft (dashed arrow) is not shown on the CE-MRA image since it is not included in the imaging volume. At the edge of the FOV (arrowhead), artery delineation is compromised by banding artifacts when using the bSSFP-based NC-MRA technique. The CE-MRA and NC-MRA scans have slightly different FOV as the imaging session was interrupted at request of the patient.